



**In-situ**

K. C. Wang, L. H. Cheng, L. Esslinger, G. T. P. Jones

Gemological Institute, China University of Geosciences, Wuhan 430074, PR China  
 Hubei Gem and Jewelry Engineering Technology Research Center, Wuhan 430074, PR China  
 School of Materials Science and Engineering, Huazhong University of Science and Technology, Wuhan 430074, PR China  
 Mechanical Engineering, University of Birmingham, Birmingham B15 2TT, UK  
 School of Electrical and Electronic Engineering, Huazhong University of Science and Technology, Wuhan 430074, PR China  
<sup>†</sup>WMG, Materials Engineering Centre, University of Warwick, CV4 7AL Coventry, UK

ARTICLE INFO

Keywords:

Titanium matrix composites  
 Carbon fiber  
 SLM  
 CVD  
 EMI

ABSTRACT

Carbon fiber (CF) reinforced titanium matrix composites (TMCs) are promising materials for aerospace applications. However, the poor interfacial bonding between the carbon fiber and titanium matrix is a major problem. In this study, a carbon fiber reinforced titanium matrix composite (CF/TMC) is fabricated by selective laser melting (SLM) of a titanium matrix with carbon fiber (CF) and carbon fiber reinforced titanium matrix composite (CF/TMC) powder. The microstructure and mechanical properties of the CF/TMC are investigated. The results show that the SLM process can effectively improve the interfacial bonding between the carbon fiber and titanium matrix. The tensile strength of the CF/TMC is 478 MPa, which is 27% higher than that of the titanium matrix. The elongation to failure is 2.7%, which is 88% higher than that of the titanium matrix. The electromagnetic interference (EMI) shielding effectiveness (SE) of the CF/TMC is 32.3 dB, which is 18 dB higher than that of the titanium matrix. The results indicate that the SLM process is a promising method for fabricating high-performance TMCs.

1. Introduction

Carbon fiber reinforced titanium matrix composites (CF/TMCs) are promising materials for aerospace applications. However, the poor interfacial bonding between the carbon fiber and titanium matrix is a major problem. In this study, a carbon fiber reinforced titanium matrix composite (CF/TMC) is fabricated by selective laser melting (SLM) of a titanium matrix with carbon fiber (CF) and carbon fiber reinforced titanium matrix composite (CF/TMC) powder. The microstructure and mechanical properties of the CF/TMC are investigated. The results show that the SLM process can effectively improve the interfacial bonding between the carbon fiber and titanium matrix. The tensile strength of the CF/TMC is 478 MPa, which is 27% higher than that of the titanium matrix. The elongation to failure is 2.7%, which is 88% higher than that of the titanium matrix. The electromagnetic interference (EMI) shielding effectiveness (SE) of the CF/TMC is 32.3 dB, which is 18 dB higher than that of the titanium matrix. The results indicate that the SLM process is a promising method for fabricating high-performance TMCs.

\*Corresponding author. E-mail address: wangkc@cgic.cug.edu.cn (K.C. Wang).

s . T , X s s ( . . , s -  
 s ) , X fl fi s  
 ( . . , l ss, f s) f 3DG. B s s, -  
 3DG ll s f l l  
 ( . . , s , s , s f l ). H , s f s  
 l l s l s ffi l  
 s l l s , f s , l N f  
 ll s s l ll f  
 , s s l 3DG s s l f -  
 s s s f s f s fi f l s 17,18 .  
 H , s f ss l l s ,  
 s l l f s s 3DG  
 l s s s l f s 19 .  
 S l l s l (SLM), s -  
 f (AM) l , s l l s f f  
 f s s / s X - s l (3D) l l s  
 s f l X s , ffi  
 fi X l f in-situ f l . T , s  
 s s SLM s s s f T ll s 20 ,  
 s l ss ll s 21 , N ll s 22 . C s s l s f l /  
 s s f l - s s s - f - -  
 s s l s . C N s s ,  
 s s s l s s f  
 CVD l s l (< 0.001 . %) -  
 ss s l f ,  
 l s l l s 23 . W l N s  
 s l l (> 0.1 . %) 17 , fi s  
 f s f X ss 24 . H , -  
 s SLM f s s ll s f s ffi  
 f s l f s s l  
 fl s l s l  
 (1000–1100 ). F f s s s ff l s  
 SLM s s ll f ll s 25 .  
 T l s , f fi s s  
 f s l - 3DG/ (3DG/C ) s -  
 s SLM s l s CVD f  
 . A ll- s - s l s  
 ll s SLM f s l l -  
 42488-7904 s888-311(SL8)-65015f

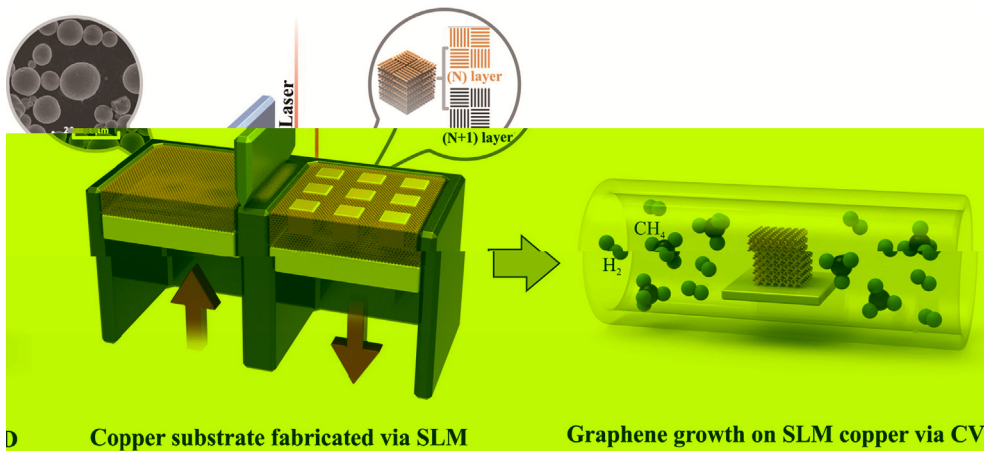


Fig. 1. SLM of copper substrate and in-situ CVD growth of graphene on SLM copper substrate.

ASTM B193-2002 (2010) and ASTM E1461-2013 (2013) standards were used to evaluate the mechanical properties of the SLM copper substrate. The tensile strength and elongation at break were measured using a universal testing machine (LFA457, GOM) with a load cell of 5 kg. The microhardness was measured using a Vickers hardness tester (LFA457, GOM) with a load of 10 g. The surface morphology was characterized using a scanning electron microscope (SEM, ZEISS) and an energy-dispersive X-ray (EDS) spectrometer. The chemical composition was analyzed using an inductively coupled plasma atomic emission spectrometer (ICP-AES, PERKINELMER). The surface energy was measured using a contact angle goniometer (CA1000, OCA). The surface roughness was measured using a surface profilometer (S11, S21, ZEISS). The surface area was calculated using the following equation:

$$S = \pi r^2 + 2\pi r h$$

where  $S$  is the surface area,  $r$  is the radius, and  $h$  is the height. The surface energy was calculated using the following equation:

$$\gamma = \frac{W}{S}$$

where  $\gamma$  is the surface energy,  $W$  is the work of adhesion, and  $S$  is the surface area. The surface roughness was calculated using the following equation:

$$R_a = \frac{1}{N} \sum_{i=1}^N |z_i - \bar{z}|$$

where  $R_a$  is the surface roughness,  $N$  is the number of data points,  $z_i$  is the height of the  $i$ -th data point, and  $\bar{z}$  is the average height. The surface area was calculated using the following equation:

$$S = \pi r^2 + 2\pi r h$$

### 3. Results and discussion

#### 3.1. Formation of SLM copper

##### 3.1.1. SLM manufacturing of copper under different line energy densities

The SLM process was carried out under different line energy densities (LED) to investigate the effect of LED on the formation of SLM copper. The LED was defined as the laser power divided by the scanning speed, as shown in Eq. (1).

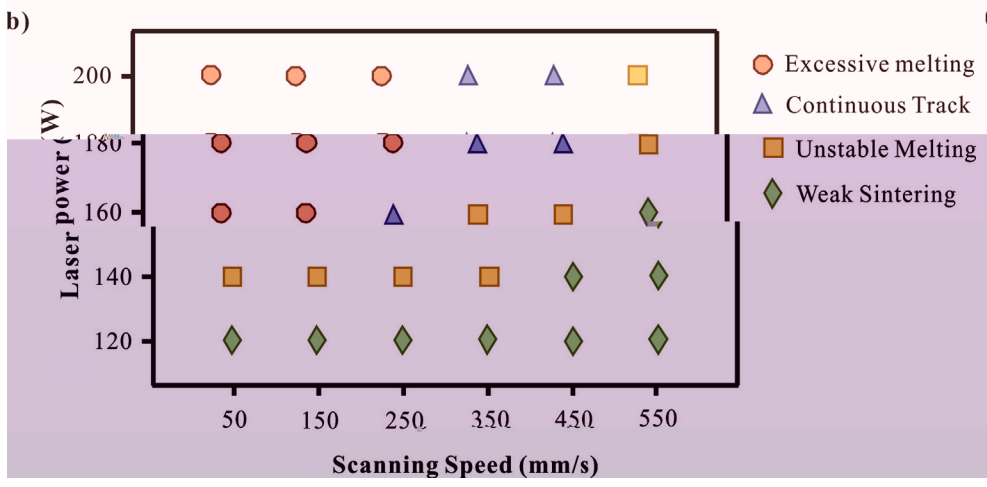
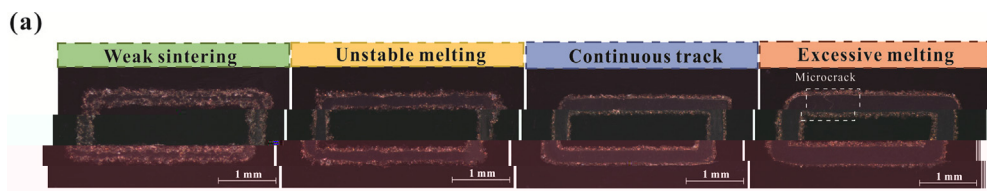


Fig. 2. (a) SEM images of SLM copper substrate under different sintering conditions. (b) Laser power versus scanning speed for different sintering conditions.

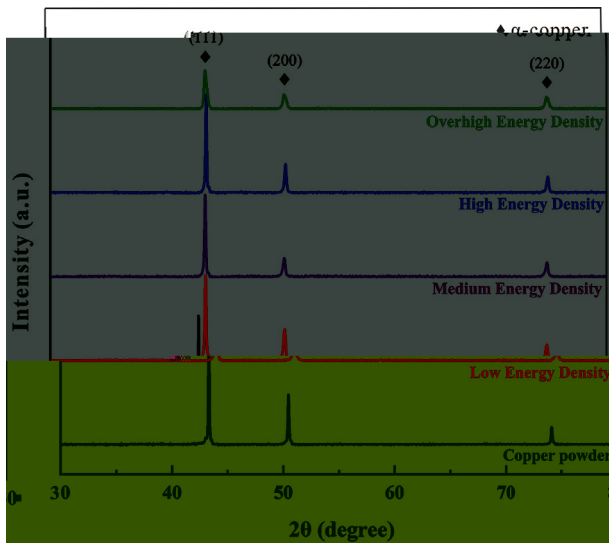


Fig. 3. RD patterns of copper powder at different energy densities.

3.1.2. Formation of anisotropic microstructure under different volumetric energy density

The XRD patterns of copper powder at different energy densities are shown in Fig. 3. The peak intensity of the (111) plane increases with the energy density, indicating the formation of a larger grain size. The peak intensity of the (200) plane also increases with the energy density, indicating the formation of a larger grain size. The peak intensity of the (220) plane also increases with the energy density, indicating the formation of a larger grain size. The peak intensity of the (111) plane is 43.32°, the peak intensity of the (200) plane is 50.45°, and the peak intensity of the (220) plane is 73.52°.

The XRD patterns of copper powder at different energy densities are shown in Fig. 3. The peak intensity of the (111) plane increases with the energy density, indicating the formation of a larger grain size. The peak intensity of the (200) plane also increases with the energy density, indicating the formation of a larger grain size. The peak intensity of the (220) plane also increases with the energy density, indicating the formation of a larger grain size. The peak intensity of the (111) plane is 43.32°, the peak intensity of the (200) plane is 50.45°, and the peak intensity of the (220) plane is 73.52°.

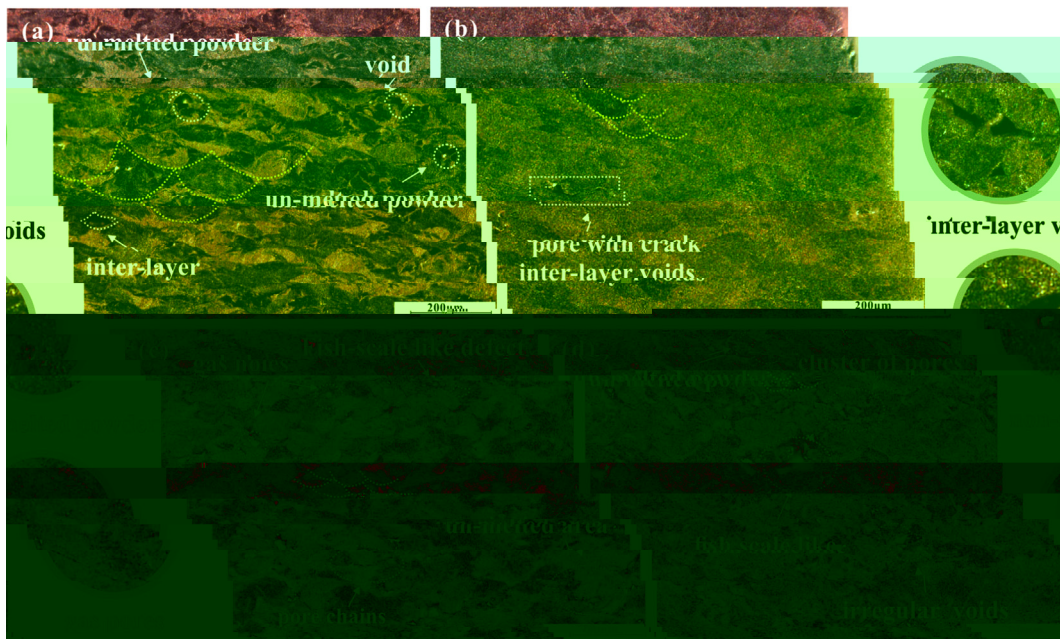


Fig. 4. SEM micrographs of SLM-processed copper powder at different energy densities.





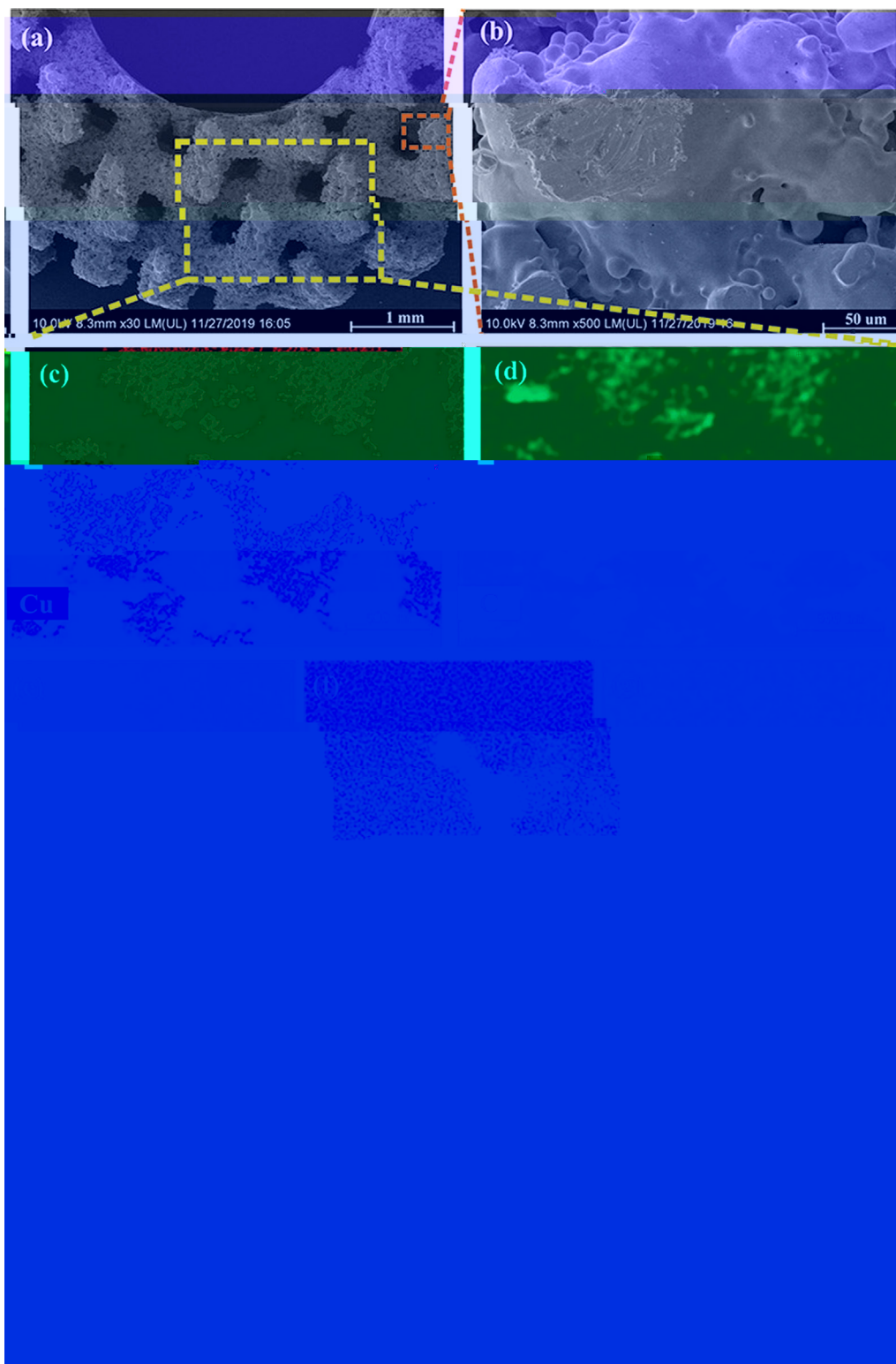


Fig. 8. (a) SEM image of 3DG/Cu porous scaffold at 30x magnification. (b) SEM image of 3DG/Cu porous scaffold at 500x magnification. (c) EDS spectrum of 3DG/Cu porous scaffold. (d) EDS spectrum of 3DG/Cu porous scaffold. The EDS map shows the distribution of Cu in the scaffold.

3.4. Thermal property and EMI shielding effectiveness of 3DG/Cu porous scaffolds

The thermal stability of the 3DG/Cu porous scaffolds was evaluated by TGA. The TGA curves show that the weight loss of the scaffolds is mainly due to the decomposition of the polymer matrix. The weight loss of the 3DG/Cu porous scaffold is 26.8% at 1000 °C, which is higher than that of the 3DG/C porous scaffold (14.8%).

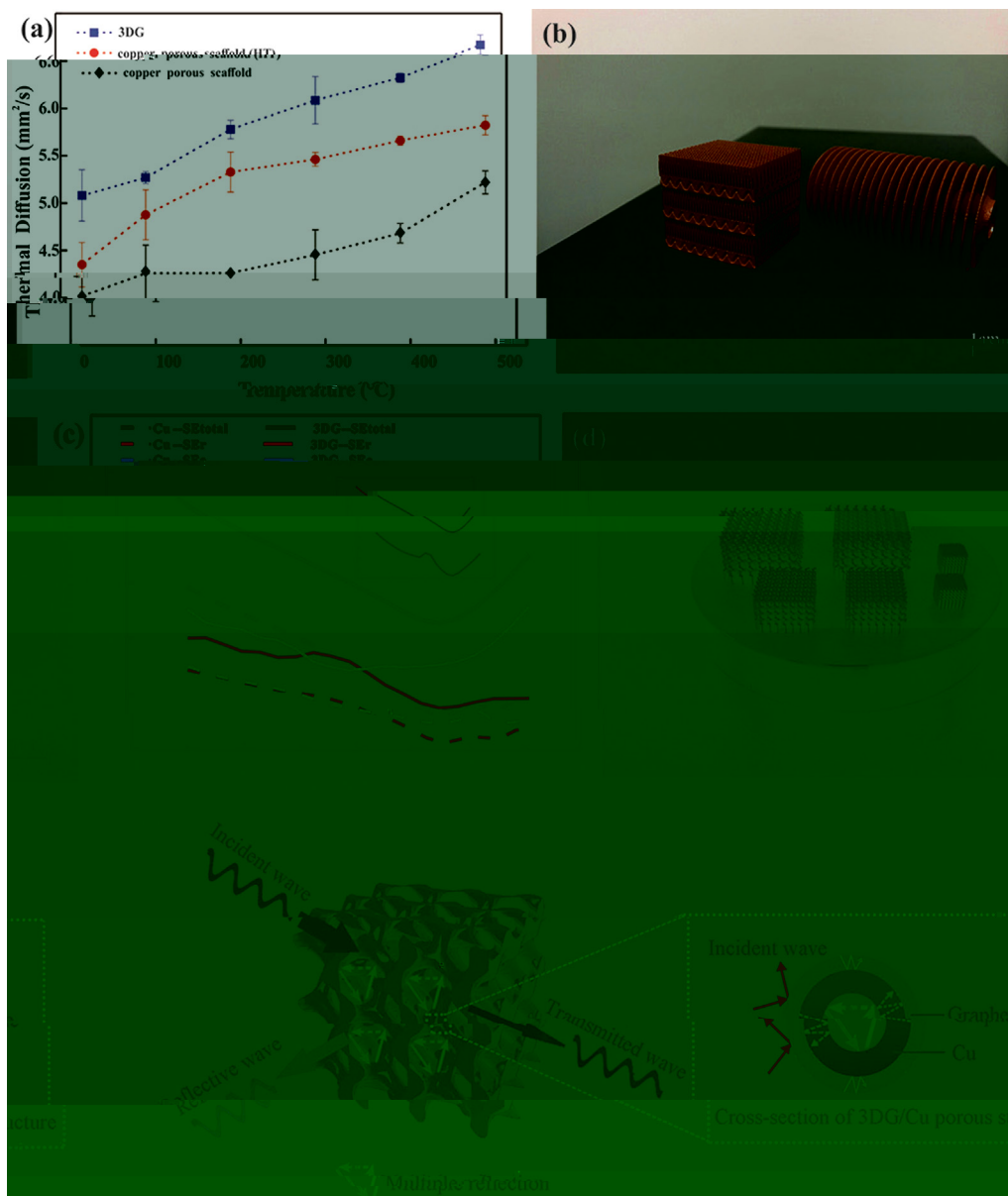


Fig. 9. P f f 3DG/C s s ff l : ( ) l ff s ; ( ) SLM s l ssff X ( -s l fl l) f - s f f s l s fi l , s f s ff l s ff s s ; ( ) S f 3DG/C EMI. (F

Table 1

Coating materials	Substrate	Method	Maximum shielding efficiency (dB)	Improvement of thermal property (%)	Ref
G	l s G	I s + f + l + l	37	-	50
G	PS	H - ss ss l + s l l	29.3	-	56
G	PMMA	S l l + l +	19	-	57
C /G	/C	S f fi + l l l	-	8.5	58
G	N	F + CVD	-	554	59
G	C -N	E l ss l + l s	20	-	60
G	C	P s + CVD	-	2.4	61
G	l s C	F - + l l	47	6.3	62
G	C	CVD + SLM	47.8	27	T s

Note: l ( l l )-PPMA, l s -PS.





Declaration of Competing Interest

T s l s fl f s

Acknowledgement

T s f ll l fi l s f
N l N l S F f C (N . 51671091, N .
51902295, N . 51675496). T
F l R s F s f C l U s s, C
U s f G s s (W ) (N . (N . CUG170677) H
P N l S F (N . 2019 CFB264).

Appendix A. Supplementary data

S l s l f l s://
/10.1016/ s s .2020.105904.

References

1 B RG, N N, M s K, M S. G : s l l f f
s s ss .P M S 2018;91:24-69.
2 B l AA, G s S, B W, C l, T l D, M F, l S
f s l l N L 2008;8(3):902-7.
3 L , H, C s M, P l H, P O, S l G, l I s X -
f l f s s f l s f f i l s l
s s. ACS A l M I f s 2016;8(36):24112-22.
4 K M, K J, J B, C , K JH, A JH. G - s - s l
s s f l l s. ACS N 2017;11(8):7950-7.
5 P , C M, H M, T M, , L D. P
s l f f - s l l l l
A l C l B 2020;262:118266-76.
6 L J, W, C LL, J SH, W G, L, l F l C-G f
l s s l .C s P A
2017;101:50-8.
7 HQ, L SW, C LH, J SH, H HQ. S l f -
- f l - s. J M C A
2018;6(42):21216-24.
8 D l s TM, S P, D s P, K J, K M, A s T, l 3D -
- s- l H l l l l s f s l s
l l l s f H . P C . P s 2017;1(4):467-70.
9 Q L, L L. T s l s l s s f l s s f l s X s .
ss l f l s f l s s f l s X s .
RSC A 2014;4(72):38273-80.
10 D , H L SP, N, W X JG. 3D X -
M S2 s : P s s -
f . C s P A 2016;90:424-32.
11 L L, W, S CO, H MK, HL, D W, l S l f ss l -s ll
- f ll s s 3D f l s fi EM -
s f . A F M 2018. s:// . /10.1002/ f .
201803938.
12 L J, P , C, R G, , N l s D, l G
s S O2 s s f l s. ACS N
2013;7(7):6001-6.
13 J SH, A l S, G A. L - s ll l s s s f l
l s. A C I E 2017;56:15520-38.
14 I , T , S K, K s M, T s T, T K, l T -
s l s s l - s l
s. PCCP 2018;20(9):6024-33.
15 S K, D N, M ll C, V s l N, E l J. T ll l
l J E l S 2002;149(8):370-7.
16 C H, S M, S WH, L G, H , Q, l P f l 3D
l X s f s s. S ll 2011;7(22):3163-8.
17 K s H, G X M, J s l H, J, W C, C M. U l -
f s l f - s l - s
. M 2019;1(4):1077-87.
18 S Q, F, , L W, L H, L , l C - l l
- s ll f s f l - f - l l
f l s l . A M 2017;29(31):1701583-90.
19 , G C, L, T H, D, W , l T s ll f -
f l f s s f
s. ACS N 2019. s:// . /10.1021/ s .9 08191.
20 C C, H , B , N J, C S, L F, l 3D s T 6A l 4V :
ff s f l s f l ;
l M D s 2019;175:107824-33.
21 S š č J, B ž č D. T ff f NB s f l -
s f 316L s ll s l s l s SLM. S f C
T l 2016;307:407-17.

22 R DC, HB, L J, L SJ, J W, R, l M s s
f T-N ll f s l l s l . M S E A-S
2020;771:138586-95.
23 L , C W, A J, K S, N J, D, l L - s s s f - l
f f l s f l s. S 2009;324(5932):1312-4.
24 C P, R WC, G LB, L BL, P SE, C HM. T - s l f l l
s . N M 2011;10:424-8.
25 J SD, D s S, G ss s L, K JP, H X JV, V s l K.
I fl f s l l s ll ss s X l
. J M P ss T l 2019;270:47-58.
26 W, H L, L , T D, C Q, F , l Eff f s l l s l
s s l , s fi
s f s s l ll . M D s 2019;170:107697-708.
27 G DD, M s W, W ss K, P R. L s f f
ll s: l s, ss s s. I M R
2013;57(3):133-64.
28 L E, T s S, C s L, F A. Eff f s l l s l (SLM)
ss s s s f 316L s
s ll s s l J M P ss T l 2017;249:255-63.
29 s , S, W , L J, W P, C , l F f l s s f
s l s s l l s l f T 6A l 4V. A l P s A: M S
P ss 2018;124:685-98.
30 L , M, S, D W, S C. I s s
s l l s l f A l S 316L s ll ss s l . M D s
2015;87:797-806.
31 L CLA, M ss S, T M, A RC, W s PJ, L PD. T ff f
f f f l s f . A M
2019;166:294-305.
32 T , K , T WQ, T J, D s s M, M l D, l R l -
s s f α/β f l -
s l T -6A l 4V. S R 2016;6:26039-48.
33 K H, T P, L NH, T SB, C CK. G f s
ss f s l l T -6A l 4V s. V l
P s P 2016;11(3):183-91.
34 R fi HK, K NV, G H, S TL, S BE. M s s l
l . J M E P f 2013;22(12):3872-83.
35 T , K , T J, V s l G, P Q , G, l A X l
s l T -6A l 4V. J A ll s C 2015;646:303-9.
36 R DA, M LE, M H , l N l - s l
l f f f s l
f s l l . A M 2011;59(10):4088-99.
37 s , f s l l s l C -2.4N -0.7S ll . J A ll s C
2018;743:258-61.
38 K S. W ll . S E 2003;23:309-48.
39 L G , G s J ff R, G s N P. E l C (111). N
L 2010;10(9):3512-6.
40 L S, C WW, C l , R ff R S. E l f
C s l l . N L 2009;9(12):4268-72.
41 W, C, , W H, SQ, L. A s l l l l -f
f s f s f s. C
2020;161:479-85.
42 F AC, M JC, S V, C s C, L M, M F, l R
s f s P s R L 2006;97(18):187401-4.
43 S , G , J SH, F PC, H HQ. F l f l
- l s fi s l l
M L 2017;200:97-100.
44 J K, H, J, C J, D . F l l f
s l f f - ll f f C -N ll CNTs.
A l S f S 2014;311:351-6.
45 R š K, M l DP, A s C, M S, S š K. X ll EMI s l
l s l s l s l
- s s f s. C s P A 2018;12:475-84.
46 S B, L , W, W. C ss l - f s f
l l s f š s l l f (EMI) s l . ACS
A l M I f s 2016;8(12):8050-7.
47 L N, H , D F, H , L , G 2016; OH ;

M 2019;34(5):489–98.

53 W B, C M, L M. R s: l - - ffi  
 l f s l l s. A M  
 2014;26:3484–9.

54 C H, W S, J , J, X , C J, l. S ff f F<sub>3</sub>O<sub>4</sub>  
 l s fl l ( l fl ) s fl s  
 ss l s l . C s P A  
 2019;121:139–48.

55 W L, J, Q. T ff f MWCNTs l -  
 s f f -MWCNTs s s. J M S : M E l  
 2015;26(3):1895–9.

56 D , P GR, H P, Q F, M B , ML. Effi l  
 f s l fl / l s s . J. M  
 C 2012;22:18772–4.

57 HB, Q, WG, H , . T - l ll l  
 f s f l f s l . ACS A l M I f s  
 2011;3:918–24.

58 S A, U ll N, T l f V. T l l f  
 l - ll s f s l s f  
 M f R 2016. s:// . /10.1051/ f /2016021.

59 P s MT, J H, R ff RS, S L. T l s - s l f -  
 s f f l l . N L  
 2012;12:2959–64.

60 J K, H, H , D . P f f - ll f f C -N ll -  
 s s l s l f . M L  
 2017;122:244–7.

61 R H, L S, B S, K TW, L DS, L HJ, l. T - s l s  
 - s s s  
 f . S R 2015. s:// . /10.1038/s 12710.  
 ss -

62 T, F SG, L , G Q, L G, R KP, l. S s l X -  
 l f s l l f  
 s s s 3D s/ ll l  
 l f . M S E A-S 2020. s:// . /10.1016/j  
 s s .2019.105670.

63 R DA, M LE, M E, H DH, M JL, M BI, l.  
 N l - s l f f s l  
 s s l f s l . A  
 M 2011;59(10):4088–99.

64 E s SF, L KG, S s VK, M IC. T l l s f . J T s  
 E l 1973;1(1):10–38.